Article:

The Tromsø programme of in situ and sample return studies of mesospheric nanoparticles

O. Havnes[(1),*], T. Antonsen[(1)] , T. W. Hartquist[(2)], Å. Fredriksen[(1)] and J. M. C. Plane[(3)]

[(1)] University of Tromsø, Institute of Physics and Technology, NO-9037 Tromsø, Norway
[(2)]School of Physics and Astronomy, University of Leeds, Leeds LS2 9JT, United Kingdom
[(3)]School of Chemistry, University of Leeds, Leeds LS2 9JT, United Kingdom

Abstract

We review some of the work performed over the past two decades with rocket-borne detectors to study mesospheric dust or nanoparticles, including meteoric smoke particles (MSPs) and water ice particles in the mesosphere. We focus on regions in which noctilucent clouds (NLCs) and polar summer mesospheric echoes (PMSEs) occur. Our primary emphasis is on several detectors designed, built and used by the Tromsø group and collaborators, and results obtained with them. These include the DUSTY, MUDD and ICON probes, the latter for which the results of laboratory tests are presented. However, we also mention, but do not address in detail, some of the investigations conducted by others and describe very briefly our preparations for sample return measurements. We consider the importance of accounting for the secondary charging occurring in detectors as nanoparticles strike them, evidence that MSPs fill up to several percent of the volume in icy particles and measurements of the size distribution of the MSPs.

*Corresponding author. Tel.: +4795106441; E-mail address: ove.havnes@uit.no

1. Introduction

Rocket-borne detectors have provided data on the nanoparticles in NLCs for over fifty years (e. g. Hemenway et al., 1964). However, the first measurements of the charge carried by mesospheric nanoparticles in NLC/PMSE layers occurred more than three decades after the studies of such particles with rocket-borne instruments began (Havnes et al., 1996). The full interpretation of the results of the charge measurements required more than another decade (Havnes and Næsheim, 2007). A variety of new instruments have been designed for the rocket payloads. The early analyses of results obtained with some such instruments have been performed, and other instruments will be flying in the next couple of years.

This paper presents a review of some of the rocket detectors developed over roughly the past two decades for studies of nanoparticles in NLC/PMSE regions. The review is not intended to be comprehensive and mainly concerns detectors designed and used by the Tromsø group and collaborators. The efforts and results of several other important groups working in the area are mentioned only in passing but are vital for progress. Indeed, the study of NLC/PMSE regions benefits greatly from the excellent cooperation between the different groups to exploit complementary techniques to achieve the best science.

Section 2 concerns the type of detector first used by the Tromsø group and collaborators to study the charge carried by NLC/PMSE nanoparticles and the results obtained with two such detectors launched in 1994. Key results (Havnes et al, 1996) are the first direct in situ detection of charged dust particles, and the demonstration of the correspondence between regions where electron bite-outs occur and those in which the negative charge carried by the nanoparticles has the greatest magnitude (Pedersen et al; 1969, Ulwick et al 1988). Another important later conclusions is that the icy nanoparticles in those regions contain substantial amounts of meteoric material in the form of smoke particles (Havnes and Næsheim 2007, Hervig et al; 2012). Section 3 contains a description of a detector first flown in 2011 and how its results have been interpreted to obtain information about the mass distribution of the meteoric smoke particles contained in the icy NLC/PMSE nanoparticles. Section 4 includes a description of tests that demonstrate the possibility of maintaining the required pressure in a vacuum chamber in a new instrument to perform in situ mass spectrometry of the single meteoric atoms and molecules that, like the meteoric smoke, are embedded in the icy nanoparticles. Section 5 contains a brief description of a detector designed to collect and return NLC/PMSE material, and section 6 concludes the paper.

2. DUSTY

The first unambiguous detections of the charge carried by mesospheric dust or nanoparticles were made with two DUSTY probes (Havnes et al., 1996), with which the influence of the nanoparticles on the mesospheric charge balance was also demonstrated. Figure 1 shows the structure of a DUSTY probe. The probe has two grids G1 and G2 at potentials +6.2 V and -6.2 V to prevent ions and electrons from reaching the bottom plate BP which is at -2 V. The NLC/PMSE particles of radius above a few nm will not be stopped by these grid potentials or be deflected away from the probe by the gas flow around the payload (Horanyi et al, 1999, Hedin et al, 2007) and will impact on the bottom plate unless they directly hit either G1 or G2. The currents to G1, G2 and BP are all sampled at a rate 2441.4 Hz, 1220.7 Hz and 1220.7 Hz

respectively. The electron current sampling rates at G1, G2 and BP were 2441.4 Hz, 1220.7 Hz and 1220.7 Hz, respectively, and each electrometer measured positive and negative currents with amplitudes in the range of 10^{-11} to 10^{-5} A.   DUSTY1/94 (ECT-02) was launched on 28 July 1994 from Andøya Rocket Range during PMSE activity but while visible NLCs were absent. When analyzing the data, Havnes et al. (1996) made most use of the currents measured at G2 and BP. They assumed that secondary charge could be produced at BP but neglected the possibility of secondary charging at G2. The analysis of the DUSTY-1 data yielded the charge density carried by dust as a function of altitude with a resolution of about a half meter. The most extreme charge density was found to be about -3000 to -4500 e/cm^3 at 85.3 to 85.7 km and at 87.4 to 87.9 km, which coincided with pronounced minima in the electron density. Havnes et al. (1996) noted an overall correspondence between the dusty layers and the PMSE regions, and Rapp and Lübken (2004) demonstrated in more detail that the most extreme charge densities associated with dust detected with DUSTY-1 were at altitudes where PMSE activity was maximal.

DUSTY-2/94 (ECT-07) was launched three days later when NLCs and PMSEs were present. Due to substantial coning of the rocket, impacts of dust happened mainly at the front grid G1 and it was found that secondary charging induced by grazing incidence collisions of the dust with this grid was very important. A number of investigators have recognized the importance of secondary charging, caused by incoming dust particles fragmenting and rubbing off electric charges from the surfaces that they impact (Havnes et al., 1996; Andersson and Pettersson, 1997; Vostrikov et al., 1997; Zadorozhny et al., 1997; Gumbel and Witt, 1998; Smiley et al., 2006; Amyx et al., 2008; Kassa et al., 2012). Havnes and Næsheim (2007) performed the first analysis to exploit the full potential of DUSTY-2 data and also reinterpreted the DUSTY-1 data with a model including secondary charging induced by collisions with one of the grids.

The reanalysis of DUSTY-1 data by Havnes and Næsheim (2007) did not lead to a significant change in the conclusions about the altitude profile of the charge density carried by dust. However, it showed that a model incorporating secondary charging occurring at G2 is consistent with the measured ratios of the currents on G2 and BP. They also considered a model that did not include secondary charging and in which the currents at G2 and CD were due entirely to the direct impact of positively and negatively charged mesospheric dust particles. This model yielded results that are in conflict with charge neutrality being approximately satisfied in the ambient atmosphere.

As a consequence of the large coning of DUSTY-2, the probe walls shielded most of G2 and BP from directly impacting mesospheric dust but did not prevent direct impacts on G1. During part of the flight the current measured at G1 was positive, which one might suppose to imply that the ambient dust was positively charged. However, the observed modulation of the current on G1 by the rotation of the spacecraft about its axis was inconsistent with the incoming dust being positively charged but was consistent with the incoming dust picking up negative charge in collisions with G1 while passing further into the probe. Havnes and Næsheim (2007) developed a detailed model of the rotational modulation of the G1 current including a parameterized fit to the secondary charging. The free parameters determined the dependence of the secondary charging on the dust particle size and angle of incidence of the collision with the G1 surface. The values of the free parameters derived from the model fits to the DUSTY-2 G1 current data indicate that the fraction of collision fragments which became charged is orders of magnitude larger than found in laboratory experiments with pure ice (Tomsic, 2001). Consequently, Havnes and Næsheim (2007) suggested that ambient icy particles were not composed of pure ice and considered what the impurities might be.

Traditionally each NLC/PMSE particle was thought to consist almost entirely of water ice (Hervig et al., 2001; Eremenko et al., 2005; Gordley et al., 2009), which possibly accumulated around a single MSP that served as the condensation nucleus (Plane, 2003; Rapp and Thomas, 2006; Plane, 2011). However, recent observations show that the NLC/PMSE particles probably act as sinks for metallic atoms injected into the upper mesosphere by meteors (Plane, 2004; Lübken and Höffner, 2004; She et al., 2006). Thus, the particles can also contain meteoric material in molecular form.

Havnes and Næsheim (2007) suggested that the impurities that they inferred to exist in the NLC/PMSE ice particles are MSPs captured during the growth of the ice particles. MSPs probably have sizes of a few nm and less (Hunten et al., 1980; Megner et al., 2008) and may consist of metallic silicates or carbonates (Plane, 2004), wüstite or magnesiowüstite (Hervig et al., 2012). In a collision in which a NLC/PMSE particle shatters, MSP fragments should survive even if water ice fragments of similar sizes do not. This should lead to the survival of orders of magnitude more small nm fragments capable of carrying a charge than a collision of a pure ice particle would.

The interpretation of measurements made during a subsequent rocket flight in which a DUSTY probe was sprayed by fragments produced in collisions of mesospheric particles with the payload body led to the same conclusion (Kassa et al., 2012). The conclusion of Havnes and Næsheim (2007) is also supported by recent satellite observations (Hervig et al., 2012) that

indicate that the ice particles in the polar mesospheric clouds (PMCs) contain MSPs filling 0.01% to 3% of the icy particles' volume.

However, Zadoroshny et al. (1997) have claimed that secondary charging occurring in the fragmentation of pure ice mesospheric particles can account for deviations of electric field measurements obtained with rocket probes and the expected true electric field properties. Unfortunately, the effects of dust impacts and secondary charging effects could not be fully isolated and identified for these probes.

DUSTY-like probes suffer the drawback that dust particles smaller than about 2 nm are probably swept away from them by the airstreams around the payloads (Horányi et al., 1999; Hedin et al., 2007). The designs of more recent dust probes (Gelinas et al., 1998; Croskey et al., 2001; Rapp et al., 2005; Rapp and Strelnikova, 2009, Robertson et al., 2009) have alleviated this problem, and the smallest dust particles are now detected. One should, however, be aware of that the measurements made with many of these probes can be affected by secondary charging effects, just as the measurements made with the DUSTY probes were. Compensation for secondary charging shows that in some cases such charging has dominated the recorded signals and swamped the electric current contributions of the charges initially carried by the ambient dust (Havnes and Næsheim, 2007; Kassa et al., 2012).

3. The MUltiple Dust Detector (MUDD)

The Tromsø group has developed MUDD in order to obtain insight into the size distribution of the MSPs suggested to be the collision fragments involved in secondary charging in probes like DUSTY1 and DUSTY2. Havnes et al. (2014) have described MUDD instruments and the first results obtained with one.

Figure 2 shows the structure of a MUDD, which has an inner diameter of 48 mm and contains 3 grids: G0, G1 and G2. G0 at the top is at the payload potential and screens other instruments from the electric field inside the MUDD. G1 has a fixed voltage of +6.2 V and stops ambient positive ions from entering the probe. The voltage of G2 is maintained at +10 V. In contrast to G0 and G1, which are designed to be "transparent" to incoming particles, G2 consists of concentric inclined metal rings that overlap slightly to prevent all incoming primary dust particles from directly hitting the bottom plate (BP) below G2. Collisions of incoming dust particles with G2 produce fragments, which should move nearly parallel to the G2 surfaces (Andersson and Pettersson, 1997, Tomsic 2001). The fragments eventually hit BP unless stopped by the electric field and air friction between it and G2. The electric potential of BP is

varied, facilitating the study of the fragment energy distribution function. The variation follows a cycle during which the BP voltage is initially +10 V and then changed to 0 V, -10 V, 0 V and then back to +10 V to start a new cycle. The voltage is maintained at each value for 0.02 seconds, during which the currents to G1, G2 and BP are read 39 times at a rate of 1920 Hz, and the probe ascends ~14 m. There is a gap of ~0.003 seconds during which currents are not read when each change of the voltage on BP occurs.

The first MUDD was part of the PHOCUS payload, launched from Kiruna on 21 July 2011 at 0701 UT. The data obtained with MST radars at Kiruna (ESRAD) showed that a persistent PMSE layer was present. The PMSE layer was also observed with radars at Tromsø (MORRO) and Andøya (MAARSY), and large NLC particles were detected with the Esrange lidar. The payload functioned nominally and reached an altitude of 108 km.

The initial step in the analysis of the data for the G1, G2 and BP currents concerns the data obtained when G2 and BP both have voltages of +10 V and involves the extraction of the leakage current due to the roughly 2% of the external electrons that reach G2 and then BP. For other BP voltages, this leakage current is zero. In regions containing no dust, the external electrons are responsible for all of the BP current and all of the G2 current. The altitude variation of the ratio of the BP current to the G2 current in such regions was fit and extrapolated into the regions where dust was abundant. Even where the dust was abundant, the ambient electrons dominated the G2 current and the multiplication of the G2 current by the ratio given by the fit should give a good approximation to the contribution of the ambient electrons to the BP current. Even so, some additional analysis to take into account the small effects of the dust on the G2 current led to a roughly one percent correction to the ambient electron contribution to the BP current. The subtraction of this contribution and the inclusion of zero point shifts to compensate for the small differences at altitudes of 79.5 to 80.5 km between the measured BP currents for different voltages yield the contribution by the dust fragments to the BP current. For BP voltages other than +10 V, the only contribution to the BP current is due to the dust fragments.

Figure 3 shows the average contributions of dust fragments to the BP current at each of the four phases of the voltage cycling. The averaging was performed over each set of 39 readouts. Green, red, black and blue lines connect the results for the phases when the BP voltage was +10 V, 0 V, -10 V and 0 V, respectively, and the potential difference, V_R, between G2 and BP was 0 V, +10 V, +20 V and +10 V, respectively. The green curve shows the total secondary current on BP due to all charged fragments, which is why it has the largest magnitude in the dusty regions of any of the curves. For most altitudes, including those above ~81.5 km in the upper parts of the PMSE layer, the red and blue curves have larger magnitudes than the black

curve. However, at ~81.4 km one sees fluctuations, which are likely due to large variations of the dust number density over lengths less than ~14 m, of the magnitudes of the red, blue and black curves relative to each other. The full error bars shown in Figure 3 correspond to twice the standard deviation of the measurements in the altitude region from 79.5 to 80.5 km. We show the error bars only for one curve, they are similar for all the others. One sees that in the upper part of the PMSE layer the difference between the red and blue curves, which both present results for times when $V_R = 10$ V, is of the same order or smaller than the error-bars. However, the differences between the red and blue curves can be markedly larger than this in the altitude region around ~81.4 km, which is consistent with the previously mentioned substantial changes in the dust density on small length scales in that altitude region.

We will refer to the contribution of dust fragments to the BP current when $V_R = 0$ as the "total fragment current". The results shown in Figure 3 can be interpolated so that the ratio, as a function of altitude, of the averaged fragment current for a value of V_R to the averaged total fragment current can be calculated. Figure 4a shows the percentage of the currents at the different V_R ranges, compared to the total fragment currents, calculated on basis of the results in Fig.3. Havnes et al. (2014) have also used a second approach to infer the fractions of the total fragment current carried by fragments with energies in different ranges. The method is aimed at making estimates of the necessary shifts of the currents at $V_R = 10$, 20 and 10 V, to make the "best" fits to the currents at $V_R = 0$ V. These shifts cannot be made directly because of the ~ 2 m gap between each voltage change. Essentially the purpose is to determine the difference between the current at the end of each phase and the start of the next phase and to minimize the square sum of all the differences in one cycle where V_R change from 0, 10, 20 and 10 V. The differences for all phase changes and the values of the total fragment current (obtained for altitudes at which $V_R = 0$) are then used to calculate the fractions as functions of altitude. The uncertainties and the absence of measurements during intervals between the ends and starts of phases complicate the calculation of the differences. In practice, a different constant current contribution is added to the fit for each phase during which V_R is non-zero. Such a constant is not added to the results for the phase in each cycle during which $V_R = 0$. If uncertainties did not exist and measurements were made continuously, these constants could be selected to construct a continuous, smooth curve from the altitude dependent results for the fragment contribution to the BP current. However, in reality the constants are selected to minimize the root mean square of the discontinuities of the constructed curve. The derived constants are then used to calculate the altitude dependences of the fractions of fragment current carried by fragments with energies in different ranges. They are shown in Figure 4b where we

now see that fragment energy distribution, also in the lower large fluctuation region, is similar to that in the much more smoothly varying upper cloud region. The total fragment size distribution (neutral plus charged), which in principle can be inferred from the results shown in Figure 4, depends on the assumption made about how the fraction of fragments carrying charge depends on fragment radius.

The relationship between the size of a fragment and its kinetic energy must be considered in order to use the results summarized in Figure 4 to probe the size distribution of the fragments. As a first step in the consideration of this relationship, we address relevant laboratory results. We then apply the knowledge gained from the laboratory studies to infer information about the fragments.

In experiments with impacting ~7 nm and smaller pure ice particles, Tomsic (2001) found that the fragment velocities depend significantly on the sizes of the scattered fragments. Following impacts at an incident angle of 70° on gold-coated surfaces, energetic (large) fragments may retain around 60-70% of the primary particle's speed. The measurements of Tomsic (2001) do not extend lower than ~100 eV for the final fragment kinetic energy, but an extrapolation of the results indicates that a fragment with an energy in the 10 to 20 eV range may retain around a third of its initial velocity. An impact on the surface of some other materials, including smooth carbon, apparently results in the fragments moving with speeds that are higher fractions of the magnitude of the primary's velocity component parallel to the surface (Tomsic, 2001). There is no information on what the velocities would be if the fragments were meteoric smoke particles, possibly with some water layers on them. Conceivably, they might have larger velocities than ice fragments due to their higher specific weight and a water coating acting as a lubricant.

As the MUDD observations were made, the primary dust particles hit the inclined surfaces of G2 with impact angles and speeds that are close to 70° and 734 m s^{-1}, respectively. The collision fragments would have continued in directions that were nearly parallel to the surfaces of G2, and we shall assume that their trajectories were inclined at angles close to 4° to the surfaces, which would imply that the velocities of all fragments were inclined by 24° to the payload axis. In the following we shall use a fragment speed v_f of 450 $\pm$ 100 m s^{-1} for all fragments. Assuming these velocities and that each charged fragment carries one negative unit charge e, we can calculate the radius r_f of the fragments stopped by the different retarding potentials. The fragments were decelerated by the electric field and by the drag force from the neutral gas within the probe. The ram pressure of the ambient neutral gas arising from the rocket's motion through led to a compression of the gas as it interacted with and entered the

probe; consequently, we use a neutral air density inside the probe of 2×10^{21} m^{-3}, which is 4 times the density at 81 km height during the summer (Rapp et al., 2001). We also assume an elevated neutral temperature of T = 600 K and the mass of a neutral molecule to be 30 amu. We calculate the minimum size of a smoke particle, with a density of 3000 kg m^{-3}, and the minimum sizes of ice particles, with a density of 1000 kg m^{-3}, that can reach BP after traveling a distance of 13.5 mm, which is the separation between the mid-plane of G2 and BP. The calculations were performed for the three fragment velocities 350, 450 and 550 m s^{-1} and for retarding potentials of 0, 10 and 20 V. One finds that if V_R = 20 V, an ice fragment with a radius r_f < 2.2±0.3 nm will not reach BP. If V_R = 10 V, an ice fragment with r_f < 1.8±0.3 nm will not reach BP. If V_R = 0 V, the drag alone will prevent an ice particle with a radius smaller than 0.5±0.04 nm from directly reaching BP. For smoke particles, the corresponding radii are r_f (20V) < 1.5±0.2 nm, r_f(10V) < 1.2±0.2 nm and r_f (0V) < 0.3±0.03 nm, respectively. Future payloads with the MUDD probes will contain up to three identical probes as those described here but with different bottom plate (BP) potentials in their cycles. This will ensure a better fragment mass resolution. We will also have that the various MUDD probes at certain phases in their electric potential cycling, will have electric potentials overlapping with those of one of the other probes. This will allow comparison between the probes and an increased accuracy. Future MUDD will also not have any gaps in the collection of data which will lead to a further significant increase in the accuracy of the determination of fragment size distribution.

4. Identification of the COntent of NLC Particles (ICON)

In addition to containing meteoric smoke (Havnes and Næsheim 2007, Hervig et al; 2012), NLC/PMSE icy particles apparently possess embedded individual atoms and molecules of meteoric material (Plane, 2004; Lübken and Höffner, 2004; She et al., 2006). Havnes et al. (2013) have described the ICON probe, which will be used to mass analyse the atomic and molecular composition of NLC icy particles. Such icy particles will be funnelled into a chamber where they will be heated sufficiently to evaporate the water.

Figure 5 shows the main components of an ICON probe. A funnel with an opening angle of 16° collects the icy particles. Many of them collide with the funnel walls and undergo some fragmentation. Unless an unexpectedly high fraction of icy material sticks to the walls, the collisions should not prevent the funnel from directing much of the icy material, and its embedded contents, towards a heated chamber where the water evaporates. Evaporated material flows from the evaporation chamber to a vacuum chamber through a pinhole, which should

remain closed until the probe ascends to within a few km of the NLC layers so that the vacuum chamber remains at a pressure below 10^{-4} torr established before launch with a removable pump and an attached ion pump. Once the pinhole is opened the permanently attached pump limits the pressure in the vacuum chamber. The contents of the vacuum chamber are mass analysed with an Extorr XT300M quadrupole Residual Gas Analyzer (RGA), which includes a programmable source of electrons that impact on the molecules and induce ionisation. With this device, a mass resolution of 1 amu over a mass range from 1 to 300 amu is achievable for a partial pressure as low as 5×10^{-14} torr, if the total pressure in the chamber is below 10^{-4} torr. However, the above ideal RGA performance require a very long sweep time which is not achievable in the short time that the rocket payload spends within and in the vicinity of the NLC/PMSE clouds. With the present RGA we therefore intend to focus on measuring on a limited amount of masses, mainly H_2O and various metals such as Fe and Na and NO_x molecules. A short sweep time will probably limit the actual partial pressure detection limit to be between 10^{-11} and 10^{-12} torr.

The partial pressure of meteoric atomic or molecular material will be governed by the rate per unit volume at which such atoms and molecules, carried by ice particles, flow into the heating chamber and the timescale on which they are removed by various loss mechanisms. The inflow rate per unit volume is given by $\alpha f_m A_f v_r N_d m_d / V_c m_w$, where α is the fraction of the ambient ice that reaches the heated chamber and will be assumed to be 0.9. f_m is the ratio of the number of meteoric atoms and molecules to the number of water molecules and will be assumed to be 4×10^{-5} (Plane 2013, priv.com). A_f, v_r, N_d, m_d, V_c and m_w are the entrance cross section of the funnel, the speed of the rocket, the ambient number density of icy nanoparticles, the typical mass of such a nanoparticle, the volume of the chamber and the mass of a water molecule, respectively. We shall assume the values of these quantities to be 3×10^{-3} m^2, 900 m s^{-1}, 8×10^7 m^{-3}, 5×10^{-19} kg, 4.4×10^{-6} m^3 and 18 amu, respectively. For the assumed values of parameters, the inflow rate per unit volume is 3×10^{16} m^{-3} s^{-1}.

Gas will be lost from the front of the chamber due to its expansion caused by the decrease in pressure as the payload rises. The removal timescale due to this process is comparable to timescale required for the payload to travel one ambient pressure scale height, which is about 5 km and which the payload traverses in about 5 s. Diffusion through the front of the chamber gives a shorter loss time, which we calculate for an assumed total number density of molecules in the chamber of 5×10^{21} m^{-3}. The ambient total number density at an altitude of 81 km is only about one tenth this, but ram pressure induced compression of the gas will occur. We assume the temperature, collision frequency corresponding to the total number density mentioned

above, molecular mass of a meteoric molecule and length of the chamber to be 300 K, 4 x 10^5 s^{-1}, 100 amu and 0.1 m, respectively. This gives a loss timescale of the order of 0.1 s.

The input rate per unit volume and loss timescale calculated above and the assumed total number density of molecules in the evaporation chamber imply that the partial pressure of the meteoric atoms and molecules would be of the order of 10^{-6} of the total pressure. For water the partial pressure should be very much higher, possibly as much as a few percent. Assuming that within the vacuum chamber these ratios would have the same value and that pumping would reduce the total pressure to 10^{-4} torr, one finds that the partial pressure of meteoric atoms and molecules could be of the order of 10 to 100 times the minimum partial pressure required for the mass spectrometer to operate with 1 amu resolution. Water molecules should be easily detectable and allow an estimate of the relative abundance of meteoric molecules in the NLC/PMSE ice particles.

To test the operation of an ICON probe, we have used a larger vacuum tank to create an environment in which the pressure was reduced to values comparable to those that the total pressure in the ICON evaporation chamber will attain as the probe flies through NLC/PMSE layers (Havnes et al. 2013). The ICON vacuum chamber pressure was initially 1.5 x 10^{-5} mbar, which was lower than the tank pressure. Once the pinhole connecting the evaporation chamber and the vacuum chamber opened, the pressure in the vacuum chamber rose even though the ICON pump attached to it operated. The procedure was performed for four larger vacuum tank pressures of 1.0, 0.5, 0.1 and 0.05 mbar, and in all tests, except for the one for which the tank pressure was 1.0 mbar, the ICON vacuum chamber pressure remained below 10^{-4} mbar. Thus, in-flight conditions in the vacuum chamber can be maintained in a range in which the RGA can operate. The results of the tests are shown for the four different tank pressures in Figure 6. A critical factor is the time for the RGA vacuum chamber content to be replaced by new gas entering through the pin hole. This time is very dependent on the ion pump capacity, vacuum chamber volume, pin hole diameter and collection chamber number density. The pinhole will be opened close to the lower edge of the NLC/PMSE cloud to ensure that the initial filling of the RGA vacuum chamber contain a maximum of ice particle material. ICON is planned to be launched in July 2015 from Andøøya Rocket Range, Norway.

5. Sample Return with the MEteoric Smoke Sampler (MESS)

A number of early attempts to sample and return NLC/PMSE particles were made (e. g. Hemenway et al., 1964, 1972; Witt, 1969; Farlow et al., 1970; Ferry and Farlow, 1972; Rauser and Fechtig, 1973, Havnes et al, 1996), but no such particles were firmly identified. The

existence of impacting particles with halo radii ranging from 100 nm to 600 nm and solid nuclei having radii between 50 and 200 nm was claimed (Hemenway et al., 1964; Ferry and Farlow, 1972). However, this claim is in conflict with early optical investigations (Gadsden and Schröder 1989) and with what is now known about the sizes of NLC/PMSE particles (von Cossart et al., 1999; Gumbel et al., 2001; Russell et al., 2009; Hervig et al., 2012). More recent attempts to return the MSPs have occurred (Gumbel, 2005, Hedin et al., 2014), but so far no conclusive results have been reported. Other types of planned smoke sampling techniques have also been presented (Reid et al., 2013)

The Tromsø group is leading the development of a new type of sample return instrument called MESS. The objective is to collect and return MSPs. The operation of MESS is based on the new model for the structure of the icy NLC/PMSE particles. As described in section 2, Havnes and Næsheim (2007) and Hervig et al. (2012) concluded that a NLC/PMSE icy particle must contain a large number of MSPs. Havnes et al. (2014) found that the volume filling factor of the MSPs to be between one tenth of a percent and several percent, but the low value seems unrealistic since it would require practically all embedded MSPs to have been released and charged when NLC/PMSE particles collided within the MUDD probe. Using the upper limit of 3% of Hervig et al. (2012) and an average size of the embedded MSPs to be 1.2 nm (Havnes et al., 2014), we find that a 50 nm NLC/PMSE particle should contain $\approx$ 2000 MSPs separated from each other by an average distance of about 8 nm.

Main problems with earlier attempts to sample and return MSPs have been contamination and the fact that the very small MSPs, with radii of a few nm and smaller, are usually deflected away from the collection surfaces by the airstreams around the payloads and their instruments. To check for possible contamination, we will launch a companion collection chamber that will be identical to the active MESS chamber but will not be opened during flight. With MESS, we plan to take advantage of the fact that the MSPs are embedded in the NLC/PMSE particles. MESS will capture NLC/PMSE particles, which will be practically unaffected by the airstream around the payload, with a funnel that will direct impacting NLC/PMSE particles into a collection chamber. This chamber will be opened at the bottom of the NLC/PMSE layers and closed above them. As the NLC/PMSE particles hit the funnel wall, they will fragment to some extent. Very small ice fragments may stick to the funnel wall and evaporate, but we expect that most of the initial NLC/PMSE particle will not fragment but instead rebound and move almost parallel to the funnel wall (Tomsic, 2001) down into the collection chamber. If we assume that $\approx$ 50% of an initial NLC/PMSE particle is collected, we can estimate the number of MSPs captured as the probe passes through a cloud of thickness H = 1000 m and having a dust number

density $N_d = 8 \times 10^7$ m^{-3} (von Cossart et al., 1999) as $N_{MSP} = 2000 N_d H A_{probe} = 4 \times 10^{11}$. The opening area of the funnel is $A_{probe} = 3 \times 10^{-3}$ m^2. The total inner surface of the collection chamber will be $\approx 10^{-3}$ m^2. If the MSPs were spread evenly over this surface the average distance between them would be ≈ 50 nm. We expect to see concentrated samples of up to a few thousand MSPs, if they remain where those parts of the NLC/PMSE particles that rebound from the funnel wall hit the collection chamber. The sample density would be smaller if some MSPs were lifted out of the collection chamber by the evaporation of the water ice in which they are initially embedded. In the worst case, all such MSPs would be removed and only the MSPs released in the first collision with the funnel walls would be deflected into the collection chamber and remain there. This would correspond to a capture of the order of ~100 MSPs for each impacting NLC/PMSE particle, leading to a total sample of 2×10^{10} MSPs. The average distance between the MSPs would then be 220 nm.

Currently, The Tromsø group is seeking funding for the recovery, with the objective of launching MESS in the next one to three years.

6. Conclusion

Much of the paper concerns recently designed instruments, relatively new measurements and ongoing efforts. However, the older data and the interpretation of them described in the paper are relevant for the interpretation and planning now underway. They scientifically underpin the ongoing work. In addition, the process by which the past work has yielded insight provides an indication of the benefits to be gained from a (stubbornly) persistent approach to the extraction of as much information as possible from the new data.

References

Amyx, K., Sternovsky, Z., Knappmiller, S., Robertson, S., Horányi, M., Gumbel, J., 2008. In-situ measurement of smoke particles in the wintertime polar mesosphere between 80 and 85 km altitude. J. Atmos. Sol. Terr. Phys., 70, 61–70.

Andersson, P. U., Pettersson, J. B. C., 1997. Ionization of water clusters by collisions with graphite surfaces. Zeitschrift für Physik D, 41, 57–62.

Croskey, C. L., Mitchell, J. D., Friedrich, M., Torkar, K. M., Hoppe,U.-P., Goldberg, R. A. 2001. Electrical structure of PMSE and NLC regions during the DROPPS program. Geophys. Res. Lett., 28, 1427–1430.

Eremenko, M. N., Petelina, S. V., Zasetsky,A.Y., Karlsson, B., Rinsland, C.P., Llewellyn, E.J., Sloan, J.J. 2005, Shape and composition of PMC particles derived from satellite remote sensing measurements. Geophys. Res. Lett., 32, L16S06.

Farlow, N. H., Ferry, G. V., Blanchard, M. B. 1970, Examination of surfaces exposed to a noctilucent cloud, August 1, 1968. J. Geophys. Res., 33, 6736-6750.

Ferry, N. H. and Farlow, G. V. 1972. Upper atmospheric dust concentrations in polar regions. Space Research XII, 1, 381-390.

Gadsden, M., Schröder, W. 1989. Noctilucent clouds., Physics and Chemistry in Space 18, Springer-Verlag.

Gelinas, L. J., Lynch, K. A., Kelley, M. C., Collins, S., Baker, S., Zhou, Q., Friedman, J. S. 1998. First observation of meteoric charged dust in the tropical mesosphere. Geophys. Res. Lett. 25, 4047–4050.

Gordley, L. L., Hervig, M. E., Fish, C., Russell, J. M., Bailey, S., Cook, J., Hansen, S., Shumway, A., Paxton, G., Deaver, L., Marshall,T., Burton, J., Magill, B., Brown, C., Thompson, E., Kemp, J. 2009. The solar occultation for ice experiment, J. Atmos. Sol. Terr. Phys., 71, 300-315.

Gumbel J., Stegman, J., Murtagh, D. P., Witt, G. 2001. Scattering phase functions and particle sizes in noctilucent clouds, Geophys. Res. Lett., 28, 1415–1418.

Gumbel, J., Waldemarsson, T., Giovane, F., Khaplanov, M., Hedin, J., Karlsson, B., Megner, L., Stegman, J., Fricke, K. H., Blum, U., Voelger, P., Kirkwood, S., Dalin, P., Sternovsky, Z., Robertson, S., Horanyi, M., Stroud, R., Siskind, D. E., Meier, R. R., Blum,

J., Summers, M., Plane, J. M. C., Mitchell, N. J., Rapp, M. 2005. The MAGIC rocket campaign: An overview, ESA Spec. Pub., 590, 139-144.

Gumbel, J., Witt, G. 1998. In situ measurements of the vertical structure of a noctilucent cloud, Geophys. Res. Lett., 25, 493–496.

Havnes, O., Antonsen, T., Fredriksen, Å., Olsen, S., Eilertsen, Y., Strømmesen, I. 2013. ICON, a mass analyzer for the ice content of NLC/PMSE particles. Proc. 21st ESA Symposium European Rocket & Balloon Programmes and Related Research, 9-13 June 2013, Thun, Switzerland (ESA SP-721, October 2013). Pp 441-444, 2013, ISSN 0379-6566.

Havnes, O., Gumbel, J., Antonsen, T., Hedin, J ., La Hoz, C. 2014. On the size distribution of collision fragments of NLC dust particles and their relevance to meteoritic smoke particles. J. Atmos. Sol. Terr. Phys.,118, 190-198, doi: 10.1016/j.jastp.2014.03.008.

Havnes, O., Næsheim, L. I. 2007. On the secondary charging effects and structure of mesospheric dust particles impacting on rocket probes, Ann. Geophys., 25, 623–637,

Havnes, O., Trøim, J., Blix, T., Mortensen, W., Næsheim, L. I., Thrane, E., Tønnesen, T. 1996. First detection of charged dust particles in the Earth's mesosphere, J. Geophys. Res., 101, 10839–10847.

Hedin, J., Gumbel, J., Rapp, M. 2007. On the efficiency of rocket-borne particle detection in the mesosphere. Atmos. Chem. Phys., 7, 3701-3711.

Hedin, J., Giovane, G.,Waldemarsson, T., Gumbel, J., Blum, J., Stroud, R.M., Marlin, L., Moser, J., Siskind, D.E., Jansson, K., Saunders, R.W., Summers, M.E., Reissaus, P., Stegman, J., Plane, J.M.C., Horányi, M. 2014. The MAGIC smoke sampler. J. Atmos. Sol. Terr. Phys.,118, 127-144, doi: 10.1016/j.jastp.2014.03.003.

Hemenway, C. L., Schmalbe, D. C., Hallgren, D. S. 1972. Stardust, Nature 238, 256-260.

Hemenway, C. L., Soberman, R. K., Witt, G. 1964. Sampling of noctilucent cloud particles, Tellus, 16, 84–88.

Hervig, M. E., Deaver, L. E., Bardeen, C. G., Russell, J. M., Bailey, S. M., Gordley, L. L. 2012. The content and composition of meteoric smoke in mesospheric ice particles from SOFIE observations, J. Atmos. Sol. Terr. Phys. 84–85, 1–6.

Hervig, M. E., Thompson, R. E., McHugh, M., Gordley, L. L., Russell, J. M., Summers, M. E. 2001, First confirmation that water ice is the primary component of polar mesospheric clouds, Geophys. Res. Lett,, 28, 971-974.

Horányi, M., Gumbel, J., Witt, G., Robertson, S. 1999. Simulation of rocket-borne particle measurements in the mesosphere, Geophys. Res. Lett., 26, 1537–1540.

Hunten, D. M., Turco, R. P., Toon, O. B. 1980. Smoke and dust particles of meteoric origin in the mesosphere and stratosphere, J. Atmos. Sci., 37, 1342–1357.

Kassa, M., Rapp, M., Hartquist, T.W., Havnes, O. 2012. Secondary charging effects due to icy dust particle impacts on rocket payloads. Ann. Geophys., 30, 433–439.

Lübken, F.-J, Höffner, J. 2004. Experimental evidence for ice particle interaction with metal atoms at the high latitude summer mesopause region. Geophys. Res. Lett., 31, L08104.

Megner, L., Siskind, DE., Rapp, M., Gumbel, J. 2008. Global and temporal distribution of meteoric smoke: a two-dimensional simulation study. J. Geophys. Res., 113:D03202.

Pedersen, A., J. Trøim, and J. Kane. 1969, Rocket measurement showing removal of electrons above the mesopause in summer at high latitudes, *Planet Space Sci., 18*, 945–947.

Plane, J.M.C. 2003. Atmospheric chemistry of meteoric metals. Chem Rev, 103:4963–4984

Plane, J.M.C. 2004. A time-resolved model of the mesospheric Na layer: constraints on the meteor input function. Atmos. Chem. Phys. 4, 627–638.

Plane, J.M.C. 2011. On the role of metal silicate molecules as ice nuclei. J. Atmos.Solar-Terr.Phys, 73, 2192-2200.

Rapp, M., Gumbel, J., Lübken, F.-J. 2001. Absolute density measurements in the middle atmosphere. Annales Geophysicae , 19, 571–580.

Rapp, M., Hedin, J., Strelnikova, I., Friedrich, M., Gumbel, J., Lübken, F.-J. 2005. Observations of positively charged nanoparticles in the nighttime polar mesosphere, Geophys. Res. Lett., 32, L23821.

Rapp, M., Lübken, F.-J. 2004. Polar mesosphere summer echoes (PMSE): Review of observations and current understanding, Atmos. Chem. Phys., 4, 2601–2633.

Rapp, M., Strelnikova, I. 2009. Measurements of meteor smoke particles during the ECOMA-2006 campaign. 1: Particle detection by active photoionization, Atmos. Sol. Terr. Phys., 71, 477– 485.

Rapp M, Thomas G.E. 2006. Modelling the microphysics of mesospheric ice particles: assessment of current capabilities and basic sensitivities. J. Atmos. Sol. Terr. Phys., 68, 715–744.

Rauser, P. and Fechtig, H. 1973. Dust measurements in the upper atmosphere during the absence of noctilucent cloud display, Space Research XIII, 2, 1127-1133.

Reid,W.,Achtert,P.,Ivchenko,N.,Magnusson,P.,Kuremyr,T.,Shepenkov,V.,Tibert, G., 2013.TechnicalNote: a novel rocket-based in situ collection technique for mesospheric and stratospheric aerosol particles.Atmos.Meas.Technol.6, 777–785, http://dx.doi.org/10.5194/amt-6-777-2013

Robertson, S., Horányi, M., Knappmiller, S., Sternovsky, Z., Holzworth, R., Shimogawa, M., Friedrich, M., Torkar, K., Gumbel, J., Megner, L., Baumgarten, G., Latteck,R., Rapp, M., Hoppe, U.-P., Hervig, M.R.. 2009. Mass analysis of charged aerosol particles in NLC and PMSE during the ECOMA/MASS campaign, Ann. Geophys., 27, 1213–1232.

Russell, J. M., Bailey, S. M., Gordley, L. L., Rusch, D. W., Horanyi, M., Hervig, M. E., Thomas, G. E., Randall, C. E., Siskind, D. E., Stevens, M. H., Summers, M. E., Taylor, M. J., Englert, C. R., Espy, P. J., McClintock, W. E., Merkel, A. W. 2009. The aeronomy of ice in the mesosphere (AIM) mission: Overview and early science results, J. Atmos. Sol. Terr. Phys., 71, 289-299.

She, C.Y., Williams, B.P., Hoffmann, P., Latteck, R., Baumgarten, G., Vance, J.D., Fiedler, J., Acott, P., Fritts, D.C., Lübken, F.-J. 2006. Simultaneous observations of sodium atoms, NLC and PMSE in the summer mesopause region above ALOMAR, Norway (69°N, 12°E). J. Atmos. Solar-Terr. Physics. 68, 93-101, DOI: 10.1016/j.jastp.2005.08.014

Smiley, B., Rapp, M., Blix, T. A., Robertson, S., Horányi, M., Latteck, R., Fiedler, J. 2006. Charge and size distribution of mesospheric aerosol particles measured inside NLC and PMSE during MIDAS and MaCWAVE 2002, J. Atmos. Solar-Terr. Phys., 68, 114–123.

Tomsic, A. 2001. Collisions between water clusters and surfaces, Dr. filos. thesis, Gothenburg University, Gothenburg.

Ulwick, J. C., K. D. Baker, M. C. Kelley, B. B. Balsley, and W. L. Ecklund. 1988, Comparison of simultaneous MST radar and electron density probe measurements during STATE, *J. Geophys. Res.*, *93*, 6989–7000.

von Cossart, G., Fiedler, J., von Zahn, U. 1999. Size distributions of NLC particles as determined from 3-color observations of NLC by ground-based lidar, Geophys. Res. Lett., 26(11), 1513–1516.

Vostrikov, A. A., Zadorozhny, A. M., Dubov, D. Y., Witt, G., Kazakova, I. V., Bragin, O. A., Kazakov, V. G., Kikhtenko, V. N., Tyutin, A. A. 1997. Ionization of water clusters by collision with surface, Z. Phys. D, 40, 542–545.

Witt, G. 1969. The nature of noctilucent clouds, Space Res., 9, 157–169.

Zadorozhny, A.M., Vostrikov, A.A., Witt, G., Bragin, O.A., Dubov, D.Y., Kazakov, V.G., Kikhtenko, V.N., Tyutin, A.A. 1997. Laboratory and in situ evidence for the presence of ice particles in a PMSE region. Geophys. Res. Lett., 24, 841-844.

Figure Captions

Figure 1. A DUSTY detector. See the text for an explanation. (From Havnes and Næsheim, 2007).

Figure 2. A MUDD detector. See the text for an explanation.

Figure 3. The average contributions of dust fragments to the BP current at each of the four phases of the voltage cycling. The value of the potential difference between G2 and BP is indicated for each curve. (From Havnes et al., 2014)

Figure 4. The fractions of the total fragment current carried by fragments with kinetic energies in the ranges of 0 to 10 eV, 10 to 20 eV and more than 20 eV. Each charged fragment is assumed to have a charge of −e. a) Results based on those presented in Figure 3. b) Results derived with the method based on the construction of a nearly continuous, smooth curve from the inferred altitude dependent values of the fragment contribution to the BP current. (From Havnes et al., 2014)

Figure 5. A schematic diagram of an ICON probe. See the text for an explanation. (From Havnes et al., 2013).

Figure 6. Laboratory tests of an ICON probe. The pressure in the vacuum chamber of the ICON probe is shown as a function of thee time that has passed since the pinhole between that chamber and the evaporation chamber was opened. The time evolution of the vacuum chamber pressure is shown for the four values of the pressure at which the environment affecting the ICON probe was maintained. (From Havnes et al., 2013).
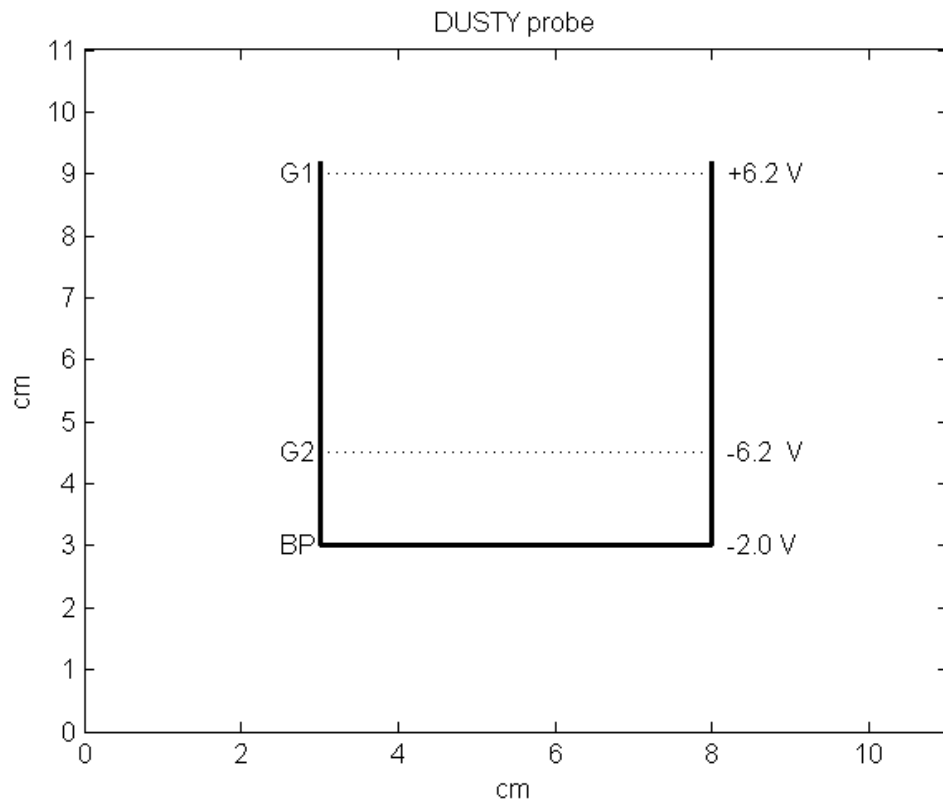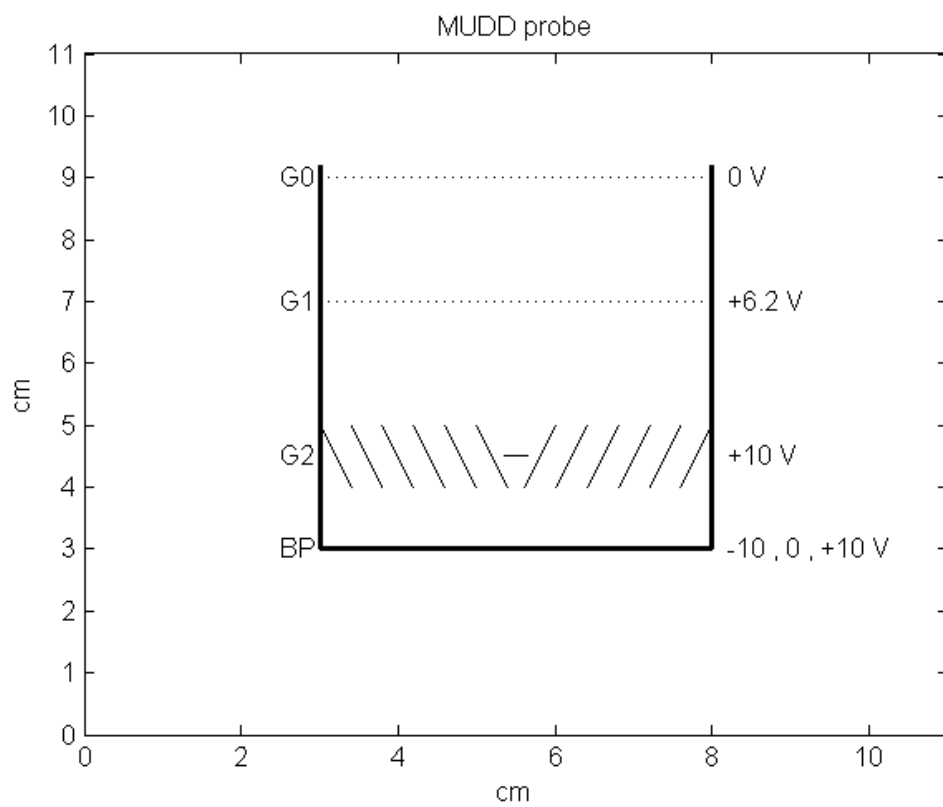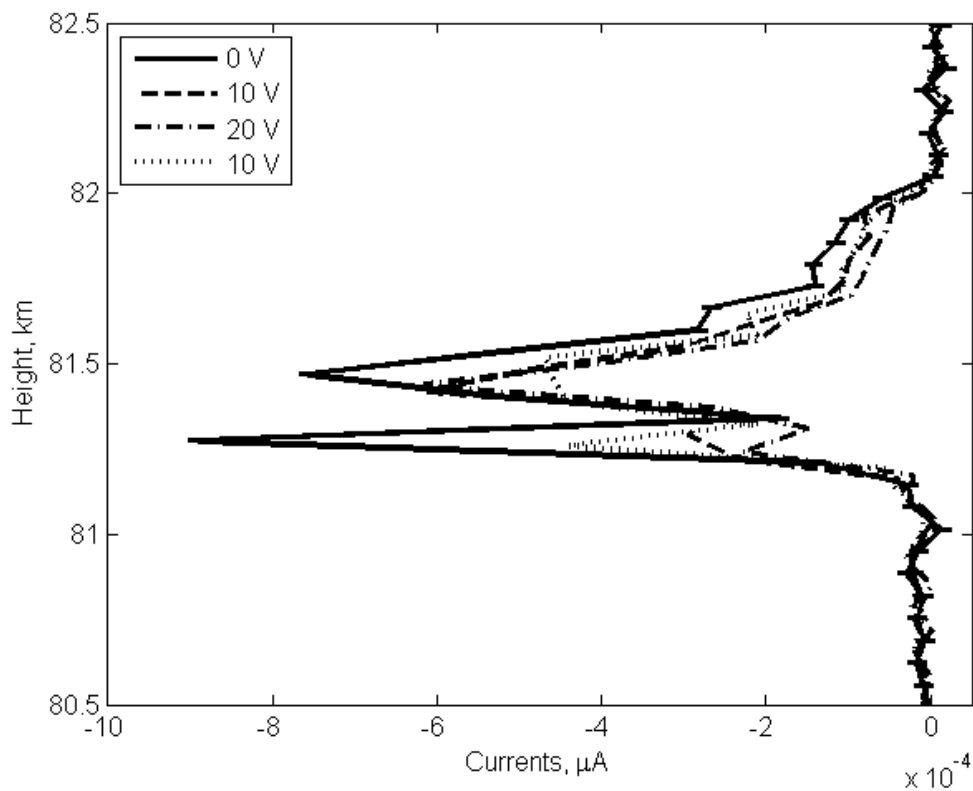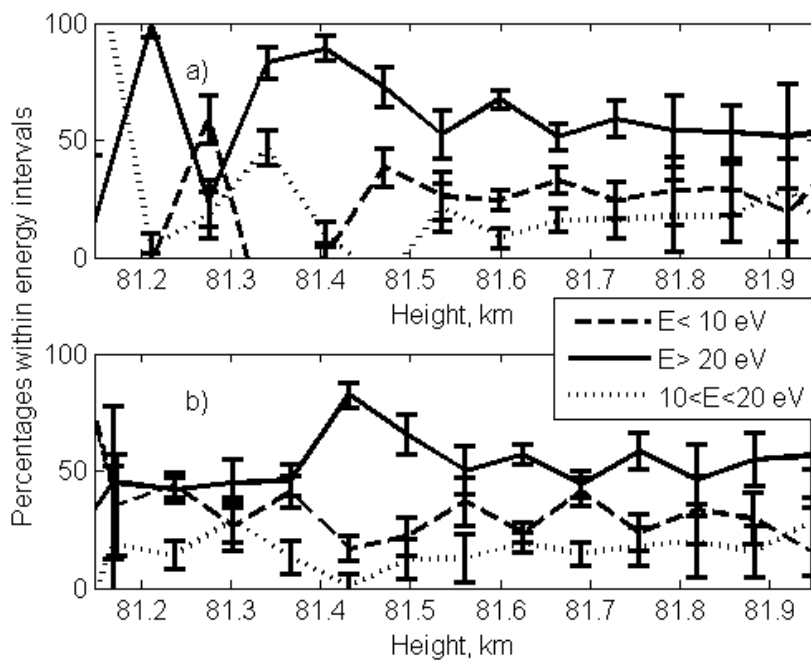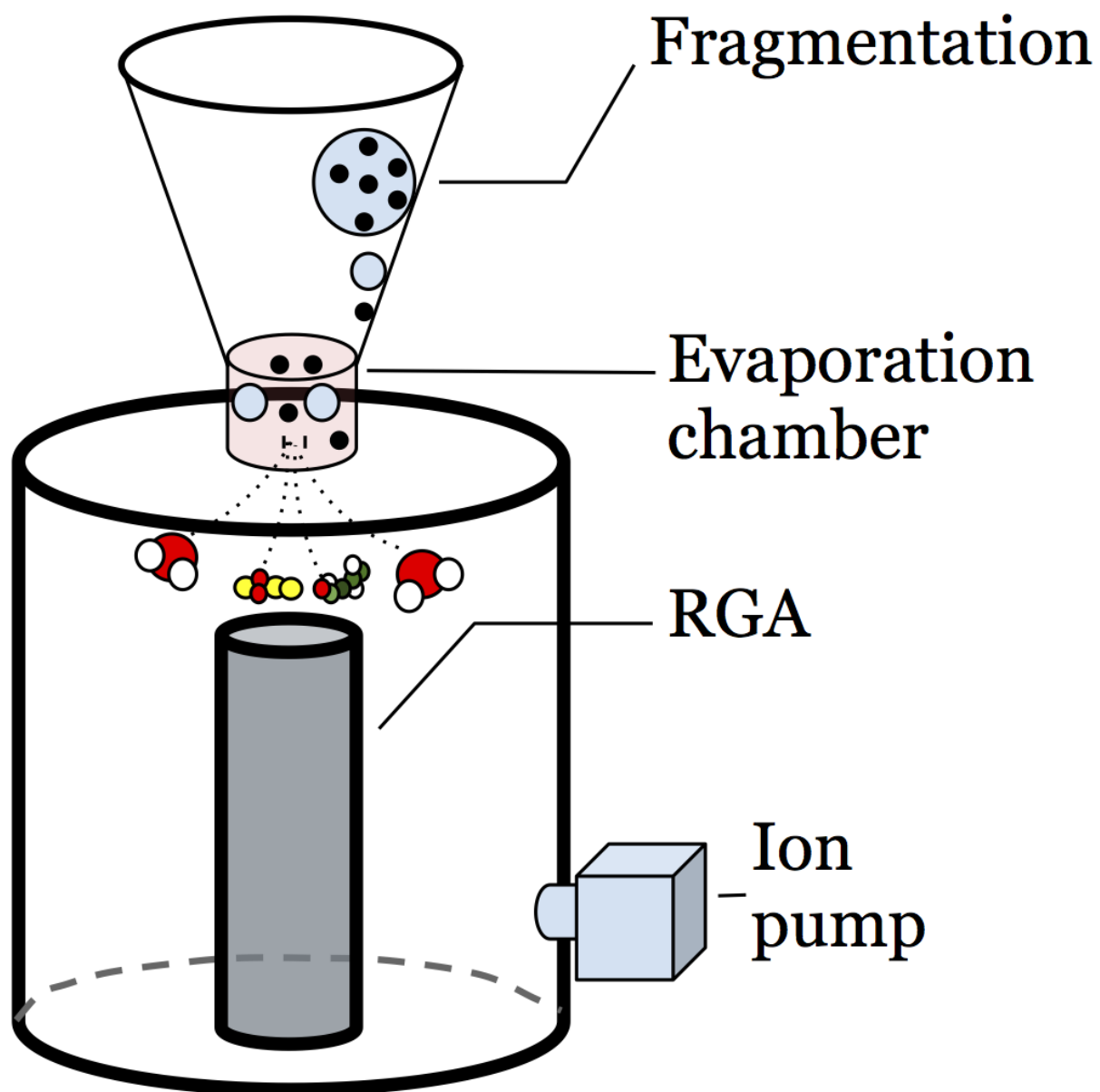
Figure 1.

Figure 2.

Figure 3.

Figure 4.

Fragmentation

Evaporation
chamber

RGA

Ion
pump

Figure 5.

Figure 6.